Materials Today Communications 15 (2018) 143–152

Contents lists available at ScienceDirect

Materials Today Communications

journal homepage: www.elsevier.com/locate/mtcomm

Development of constitutive material model of 3D printed structure via FDM

Madhukar Somireddy[a,*], Aleksander Czekanski[a], Chandra Veer Singh[b]

[a] Department of Mechanical Engineering, York University, Toronto, ON, M3J 1P3, Canada
[b] Department of Materials Science and Engineering, University of Toronto, Toronto, ON, M5S 3E4, Canada

ARTICLE INFO

Keywords:
FDM
Constitutive behavior
Build orientation
Laminate mechanics
Mesostructure
Numerical homogenization

ABSTRACT

The present paper develops the constitutive material models of the 3D printed parts via fused deposition modeling. Additive manufacturing of a part results in a complex microstructure which depends on the process parameters and build orientation. Consequently, anisotropy is introduced into the material properties. The mechanical behavior of the printed parts is governed by the constitutive behavior of the material. Therefore, the stiffness matrix of the material of the final printed part needs to be estimated for accurately capturing their behavior. The constitutive material modeling of the printed parts using numerical homogenization procedure is emphasized in this work. The present simulation models can capture the influence of build orientation, printing direction and layer thickness on the material behavior of the printed parts. Then, the influence of layer deposition in printing of differently oriented parts of the structure on the material behavior is investigated. It is revealed that the material behavior of different parts of the structure is not same and is dependent on the build orientation of the parts and also their thickness. This work aids the computation of elastic moduli and also selecting of the correct constitutive material model of the printed parts for stress analysis.

1. Introduction

Additive manufacturing (AM) techniques which fabricate a 3D part by layer upon layer deposition of the material and the associated techniques have risen in popularity in recent years [1]. These fabrication techniques have broad applications in the field of mechanical, aerospace and biomedical engineering [2]. Parts with complex geometry can be 3D printed with less effort and time when compared to other conventional machining processes. However, the build volume of AM machines is still a limiting factor for printing larger parts. The metal additive manufacturing industry has already found a way to accommodate large part sizes in the mass production of jet engines parts [3]. In near future, these AM processes will be responsible for a major change in the design of materials as well as components. The AM techniques allow for manufacturers to tailor material properties by designing the microstructure of a material. The material properties of the final printed part differ from initial material properties used for printing and these changes in the mechanical properties were addressed by Kotlinski [4]. The difference in the material properties after printing is complete is due to changes in the microstructure that are taking place during layer by layer deposition while building a part. The variation in the material properties should be taken into consideration when measuring the final properties, which are useful in the design and analysis of the parts. That means the stiffness matrix should have the final material properties of the printed part to accurately capture its mechanical behavior during finite element stress analysis. Therefore, the final mechanical properties of the material of the printed part need to be calculated for effective design and analysis of the parts subject to different loads.

A material extrusion process also known as fused deposition modeling (FDM, Stratasys Ltd.), an AM technique, fabricated parts are considered in this work. The layers of the printed part behave as an orthotropic material even though the initial filament material is isotropic. This means, the roads in a layer act as fibers in a lamina. Classical laminate theory available for the laminates can be employed for characterizing the behavior of the printed parts [5]. The quality of the printed parts depends on the process parameters of the FDM process [6]. Furthermore, the mesostructure of the printed parts is governed by the process parameters such as raster angle, layer thickness, air gap between the adjacent roads and infill pattern and density. The mesostructure of the printed part will have the fibers and voids. The presence of voids in the mesostructure of prints negatively impacts the mechanical properties of the part [7]. The properties of the part can be improved by minimizing presence of voids and improving the quality of the bonding between the fibers. The process parameters such as raster angle and air gap significantly influence the mechanical properties of the parts [8–10]. Furthermore, the dependence of mechanical properties of the printed part on the raster angle for different load cases was

* Corresponding author.
E-mail address: madhukar@yorku.ca (M. Somireddy).

https://doi.org/10.1016/j.mtcomm.2018.03.004
Received 12 February 2018; Received in revised form 7 March 2018; Accepted 8 March 2018
Available online 09 March 2018

studied in several recent studies [11–17]. The mechanical properties of the parts are influenced by bonding formation between the adjacent fibers and as well layers during the deposition of material [18,19]. The parts can be 3D printed in any orientation and the build orientation of a part is decided by the user while generating the G code for printing. The material deposition strategy is generated by the slicer tool based on orientation of the part on substrate of the printer and further, it influence the properties of the part [5]. An orthotropic material behavior was assessed by conducting experiments on the parts built in different orientations [20,21]. The build time for printing and also surface quality depends on the build orientation of the part [22,23]. The experimental work [20–29] reveals the significance of build orientation and raster angle on the properties of the printed parts. The computational work [30–32] on the material behavior of the printed part is limited and further exploration is required using multiscale models.

As discussed earlier FDM printed parts behave as laminated composite structure and Researchers [33,34] carried out experimental work for characterizing the mechanical behavior of the printed parts and also verified with laminate theory results. However, the aforementioned works are based on experimental work and did not consider internal features of the mesostructure of the printed parts while calculating their final material properties. Additionally, the work available only considers calculation of the elastic moduli for a constitutive matrix of plane stress case. The effect of the build orientation in the calculation of stiffness matrix and in the characterization of mechanical behavior of the printed parts using laminate theory is not taken into consideration. From the previous works, it is evident that the build orientation influences the material properties of the printed parts. Therefore, the variation in the material behavior due to build orientation should be considered in the characterization of mechanical behavior of the parts. Moreover, the computation of stiffness matrix of the material of the printed part accounting the build orientations using numerical multiscale models is an unexplored research area. The present paper addresses the computation of constitutive matrix by considering the build orientation of the parts using numerical homogenization. Initially, the effect of build orientation of the part on its mechanical properties is described. Then anisotropy in the material properties of the printed L-bracket structure due to deposition strategy in different parts of the structure is explained. The layers deposited along the thickness of the geometry of the part treated with laminate theory for characterization of their material behavior. Then the layers deposited across the thickness of the geometry of the part due its build orientation are characterized with orthotropic material behavior. Computation of mechanical properties of the material of the final printed part using homogenization method is explained. Influence of build orientation on the constitutive material behavior of the differently oriented parts of the structure is investigated.

2. Effect of build orientation of the part on its material behavior

The material deposition strategy in FDM, shown in Fig. 1. The material behavior of the printed part depends on the fiber orientation in the layers, stacking sequence of layers and on its build orientation [15,27]. The effects of fiber orientation and stacking sequence of layers in a 3D printed part are considered in the laminate modeling. However, the effect of build orientation of the part on material behavior cannot be accounted for using laminate theory and therefore its influence on the material properties of the printed part is extensively discussed in this work.

A three-dimensional part can be oriented on different surfaces of the part on the substrate of the printer. For example, a rectangular plate of having thickness (t) can be oriented in three different ways as shown in Fig. 1. In the first case, (Fig. 1a), the surface ABCD of the plate is lying on the substrate and is commonly known as orienting the part on the *flat* surface. The other two cases are *edge* and *upright* orientations, where the plate is oriented on its surface CDEF and BCFG respectively as shown in the Fig. 1b and c. The lamina material behavior of the layers of the 3D printed part is due fiber orientation and layer upon layer deposition. It is known from the previous experimental works [20,21] that the material behavior of the printed part is influenced by its build orientation. Therefore, the behavior of the above cases would be different, since the deposition of layers is not same. In the *flat* orientation, the layers are deposited along the thickness of the plate, where as in other cases; *edge* and *upright* orientation, the layers are deposited along width (W) and length (L) of the plate. The laminate modeling is done on midsurface of the parts. The laminate plate theory can be used for characterizing the mechanical behavior of the printed part in which the layers are deposited in only the thickness direction. That means the laminate theory can only capture the actual mechanical behavior of first case since, the layers are deposited in the thickness direction. The layers are not deposited in the same direction of the mid-surface in other two cases, as seen in Fig. 1b and c and therefore, the mechanical behavior of these cases cannot be captured using laminate modeling. It is clear that the constitutive material behavior of the printed part is dependent on the build orientation, therefore the actual constitutive material behavior of the printed parts with different orientations needs to be fully considered to account for the final material behavior in the stress analysis. The material behavior of the parts built with *edge* and *upright* position would be similar, since the layers are deposited across the thickness in both cases. Detailed discussion on the effect of build orientation on mechanical properties of the printed parts is presented in further work of the paper.

The structures used in real applications will have more than one simple geometrical shape. Let us consider an L bracket structure for 3D printing via FDM, as shown in Fig. 2. It has two different parts; horizontal plate and vertical plate. The horizontal plate is lying in the x-y plane whereas the vertical plate is in y-z plane. Now consider the case

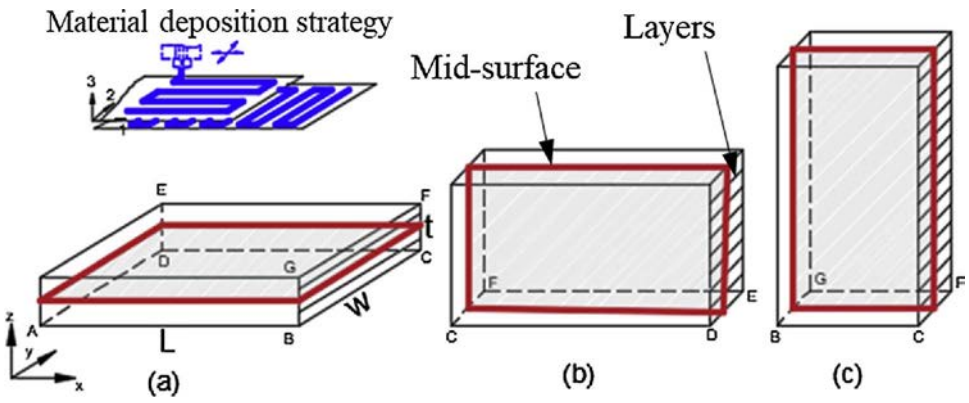

Fig. 1. Build orientations of the plate, (***a***) flat, (***b***) edge, and (***c***) upright.

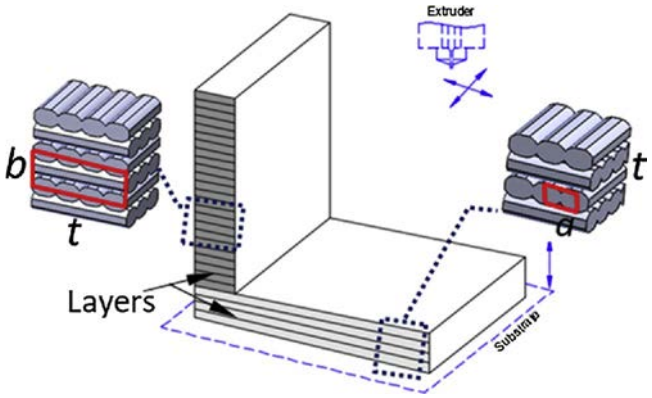

Fig. 2. 3D printed L bracket structure with its mesostructure.

where the L bracket is printed on the substrate of the printer as shown in Fig. 2. This means the build orientation of two different parts, horizontal and vertical plate, of the L bracket is different and therefore, as discussed earlier their material behavior would be different. The build orientation of horizontal plate is *flat* and the vertical plate is *upright*. The constitutive material behavior of the horizontal plate can be captured using laminate modeling, but not for the vertical plate. However, it is clear from experimental work [20,21,25,27,35] that the material behavior of printed parts in *upright* orientation is orthotropic. Therefore, constitutive material behavior of an orthotropic material can be used for characterizing the mechanical behavior of such cases. The constitutive matrix of the printed parts with different orientations is to be computed for accounting their material behavior in the analysis. This can be computed from the mesostructure of the printed part using homogenization technique [36]. The meostructure of the horizontal and vertical plate of the printed L bracket structure, shown in Fig. 2, would be considered for homogenization of the material.

3. Constitutive material behavior of printed parts

Let us consider the constitutive behavior of the two plates of the 3D printed L bracket structure for considering their material behavior in the finite element stress analysis. The layers in the horizontal plate are thin and behave as orthotropic material, and therefore, orthotropic constitutive relation for plane stress case would be considered. Then the horizontal plate can be treated as laminated plate and therefore, the classical laminate theory can be employed to account its material behavior in the analysis of the plate.

The constitutive relation for an orthotropic material is given as

$$\begin{Bmatrix}\sigma_{11}\\ \sigma_{22}\\ \sigma_{33}\\ \tau_{12}\\ \tau_{13}\\ \tau_{23}\end{Bmatrix} = \begin{bmatrix} C_{11} & C_{12} & C_{13} & 0 & 0 & 0\\ C_{12} & C_{22} & C_{23} & 0 & 0 & 0\\ C_{13} & C_{23} & C_{33} & 0 & 0 & 0\\ 0 & 0 & 0 & C_{44} & 0 & 0\\ 0 & 0 & 0 & 0 & C_{55} & 0\\ 0 & 0 & 0 & 0 & 0 & C_{66}\end{bmatrix}, \text{in matrix form } \{\sigma\} = [\boldsymbol{C}]\{\varepsilon\} \begin{Bmatrix}\varepsilon_{11}\\ \varepsilon_{22}\\ \varepsilon_{33}\\ \gamma_{12}\\ \gamma_{13}\\ \gamma_{23}\end{Bmatrix} \tag{1}$$

where C_{ij} are elements of the constitutive matrix $\boldsymbol{C}$ with *Voigt* notation. The strain-stress relation for an orthotropic material by inverting Eq. (1), written as

$$\{\varepsilon\} = [\boldsymbol{S}]\{\sigma\} \tag{2}$$

where $\boldsymbol{S}$ is compliance matrix and coefficients of the matrix are

$$S_{11} = \frac{1}{E_1},\ S_{12} = -\frac{\nu_{12}}{E_2},\ S_{13} = -\frac{\nu_{13}}{E_1},\ S_{22} = \frac{1}{E_2},\ S_{23} = -\frac{\nu_{23}}{E_2},\ S_{33} = \frac{1}{E_3},\ S_{44} = \frac{1}{G_{12}},\ S_{55} = \frac{1}{G_{13}},\ S_{66} = \frac{1}{G_{23}} \tag{3}$$

The coordinate system *1*, *2* and *3* is a lamina (local) coordinate system; axis *1* is along the fiber, axis *2* is transverse to the fiber and axis *3* is normal to the *1-2* plane which means along thickness of the layer. The coefficients C_{ij} of the $\boldsymbol{C}$ matrix for an orthotropic material are obtained by inverting the $\boldsymbol{S}$ matrix. The elastic constants required to describe an orthotropic material are; the Young's moduli of a layer along axis *1*, *2* and *3* respectively E_1, E_2, E_3, the shear moduli G_{12}, G_{13}, $G_{23}$and the Poisson's ratios ν_{12}, ν_{13}, ν_{23}. Also, the relation $E_i\nu_{ji} = E_j\nu_{ij}$ (no sum on i and j) for i, j = 1,2,3 and $i \neq j$ holds for orthotropic materials. For a transversely isotropic material, the elastic moduli in lateral and transverse direction are same.

Each layer is a thin plate and therefore the layer considered as a plane stress problem in the analysis. The strain-stress relation for a lamina under a plane stress case obtained from Eq. (2) by setting $\sigma_{33} = 0$, $\tau_{23} = 0$, $\tau_{13} = 0$ and is written as

$$\begin{Bmatrix}\varepsilon_{11}\\ \varepsilon_{22}\\ \gamma_{12}\end{Bmatrix} = \begin{bmatrix} S_{11} & S_{12} & 0\\ S_{12} & S_{22} & 0\\ 0 & 0 & S_{44}\end{bmatrix}\begin{Bmatrix}\sigma_{11}\\ \sigma_{22}\\ \tau_{12}\end{Bmatrix} \tag{4}$$

The coefficients of compliance matrix $\boldsymbol{S}$ are available in Eq. (3). The plane stress reduced constitutive relation for an orthotropic material is obtained by inverting Eq. (4). The constitutive relation of thin orthotropic layer is given as

$$\begin{Bmatrix}\sigma_{11}\\ \sigma_{22}\\ \tau_{12}\end{Bmatrix} = \begin{bmatrix} Q_{11} & Q_{12} & 0\\ Q_{12} & Q_{22} & 0\\ 0 & 0 & Q_{44}\end{bmatrix}\begin{Bmatrix}\varepsilon_{11}\\ \varepsilon_{22}\\ \gamma_{12}\end{Bmatrix} \tag{5}$$

where the Q_{ij} are coefficients of the plane stress reduced stiffness matrix $\boldsymbol{Q}$, and given by

$$Q_{11} = \frac{S_{22}}{S_{11}S_{22}-S_{12}^2} = \frac{E_1}{1-\nu_{12}\nu_{21}},\ Q_{12} = \frac{S_{12}}{S_{11}S_{22}-S_{12}^2} = \frac{\nu_{12}E_1}{1-\nu_{12}\nu_{21}}$$
$$Q_{22} = \frac{S_{11}}{S_{11}S_{22}-S_{12}^2} = \frac{E_2}{1-\nu_{12}\nu_{21}},\ Q_{44} = \frac{1}{S_{44}} = G_{12} \tag{6}$$

Note that the reduced stiffness matrix's components involve only four independent material constants, E_1, E_2, ν_{12}, and G_{12}. The global coordinate system (x,y,z) for a laminate plate and local coordinate system (*1*,*2*,*3*) for a lamina are considered.

Strains of the laminate from classical laminate theory is written as

$$\begin{Bmatrix}\varepsilon_{xx}\\ \varepsilon_{yy}\\ \gamma_{xy}\end{Bmatrix} = \begin{Bmatrix}\varepsilon_{xx}^0\\ \varepsilon_{yy}^0\\ \gamma_{xy}^0\end{Bmatrix} + z\begin{Bmatrix}k_{xx}\\ k_{yy}\\ k_{xy}\end{Bmatrix},\ \{\varepsilon\} = \{\varepsilon^0\} + z\{k\} \tag{7}$$

where ε_{xx}^0 and ε_{yy}^0 are mid-plane strains in the laminate; γ_{xy}^0 is the mid-plane shear strain in the laminate; k_{xx} and k_{yy} are bending curvature in the laminate; k_{xy} is the twisting curvature in the laminate and z is the distance from the mid plane in the thickness direction.

The constitutive relation for a laminate is written as

$$\{\sigma\} = [\overline{\boldsymbol{Q}}]\{\varepsilon\} \tag{8}$$

where $\overline{Q}_{ij}$ are transformed material constants, the elements of $\overline{Q}_{ij}$ are given as

$$[\overline{\boldsymbol{Q}}] = [T]^{-1}[\boldsymbol{Q}][T]^{-T} \tag{9}$$

where $[T]$ is a transformation matrix [34].

The Eq. (8) is constitutive relation for the horizontal plate based on laminate modeling and is useful to account the constitutive material behavior in the stress analysis. Now consider the constitutive material behavior of the vertical plate, which is printed in *upright* orientation. The build orientation of this plate is different from the horizontal plate and therefore, the material behavior is not same as that of a horizontal

plate. As discussed earlier, the layer deposition is not in its thickness direction. Therefore, the constitutive relation of the laminate (Eq. (8)) cannot be applied to vertical plate. Also, the plane stress assumption for constitutive relation is not true for this vertical plate, as thin layers are not aligned with the mid-surface of the plate. However, the material behavior of the printed plate in *upright* orientation is orthotropic in nature and therefore, an orthotropic constitutive relation (Eq. (1)) can be used in the stress analysis. The stiffness values in the constitutive matrix of the orthotropic material are unknown and are to be computed to account the material behavior in the stress analysis of the part. The computation of stiffness values of the constitutive matrix of the printed part can be done using numerical homogenization procedure. The following section covers the constitutive material modeling of the horizontal and vertical plate of the L bracket structure using homogenization technique.

3.1. Homogenization for printed parts

The effective constitutive matrix of the material of the printed plates is calculated from the known properties of virgin material used for printing the plates. The printed part is considered as continuum. A small volume of material, represents the periodic architecture of the material of the printed plate is considered for numerical homogenization and this material is called the Representative Volume Element (RVE). The prediction of effective constitutive matrix of the materials from its constituent's properties and geometrical features of the microstructure is known as *homogenization*.

The RVEs of the horizontal plate and vertical plate, shown in Fig. 3a and b, and are taken from the mesostructure of the plates as seen in Fig. 2. The RVE of the horizontal plate is taken only from the single layer of the plate, as marked region '***a***' in Fig. 2 and then the constitutive matrix of the layer can be computed using homogenization. Then, the matrix is useful in the constitutive relation of the laminate for characterizing the material behavior of the horizontal plate. As we know that the laminate theory cannot be applied for the vertical plate, the RVE of the vertical plate cannot be taken from single layer. The RVE of the vertical plate is the marked region '***b***' in the mesostructure of the plate in Fig. 2. The RVE of this plate represents the fibers of the three adjacent layers. Then the homogenization is employed to calculate the effective constitutive matrix of printed vertical plate.

In the homogenization method, the RVE is treated as a macroscopically homogeneous orthotropic material. The stresses σ_{ij} and strains ϵ_{ij} are the local fields at a point in the RVE. In a macroscopically homogeneous RVE, the macroscopic fields such as average stress $\bar{\sigma}_{ij}$ and average strains $\bar{\varepsilon}_{ij}$ are computed by averaging the local stresses and strains over the volume of RVE (V_{RVE}), respectively and are given as

$$\bar{\sigma}_{ij} = \frac{1}{V_{RVE}} \int_V \sigma_{ij}(x_1, x_2, x_3)\, dV, \quad \bar{\varepsilon}_{ij} = \frac{1}{V_{RVE}} \int_V \varepsilon_{ij}(x_1, x_2, x_3)\, dV \tag{10}$$

The strain energy U^* stored in the heterogeneous RVE of the volume V_{RVE} is

$$U^* = \frac{1}{2} \int_{V_{RVE}} \sigma_{ij}\varepsilon_{ij}\, dV \tag{11}$$

The strain energy calculated for homogeneous RVE using homogenized modulus is

$$U = \frac{1}{2}\bar{\sigma}_{ij}\bar{\varepsilon}_{ij} V_{RVE} \tag{12}$$

The main idea of homogenization model is to find globally homogeneous medium equivalent to the original microscopically heterogeneous material, where the strain energy stored in both systems is approximately same. That means

$$U^* = U \tag{13}$$

Substituting Eq. (12) into Eq. (13)

$$U^* = \frac{1}{2}\bar{\sigma}_{ij}\bar{\varepsilon}_{ij} V_{RVE} \tag{14}$$

The elastic constitutive relation of the material for a homogenized RVE is given as

$$\{\bar{\sigma}\} = [C]\{\bar{\varepsilon}\} \tag{15}$$

where [***C***] is the effective constitutive matrix of the orthotropic material and is equal to $[\boldsymbol{S}]^{-1}$ as mentioned earlier. Upon substituting Eq. (15) in Eq. (14), then we have

$$U^* = \frac{1}{2}\{\bar{\varepsilon}\}^T [C]\{\bar{\varepsilon}\} V_{RVE} \tag{16}$$

The unknown elements in the constitutive matrix can be calculated by solving for different load cases. The strain energy (U^*) of the RVE for a deformation mode is obtained from the simulation using Eq. (11) and then the corresponding unknown stiffness value of the constitutive matrix is calculated. The average strains are obtained from applied boundary displacements (u_i) on RVE and the average strains in Eq. (10) can be converted as

$$\bar{\varepsilon}_{ij} = \frac{1}{V_{RVE}} \int_{S_1} (u_i n_j + u_j n_i)\, dS_1 \tag{17}$$

where S_1 denotes the outer boundary of the RVE. In case of pure deformation, the tensorial shear strain ε_{ij} and the engineering total shear strain is given as

$$\gamma_{ij} = \varepsilon_{ij} + \varepsilon_{ji} = 2\varepsilon_{ij} \tag{18}$$

Boundary conditions: Periodic microstructure is present in the printed parts and therefore, the RVE is subjected to periodic boundary conditions. These conditions represent the continuum of the physical body. The displacement field on the boundary of the RVE can be expressed as

$$u_i(x_1, x_2, x_3) = \bar{\varepsilon}_{ik} x_k + u_i^*(x_1, x_2, x_3) \tag{19}$$

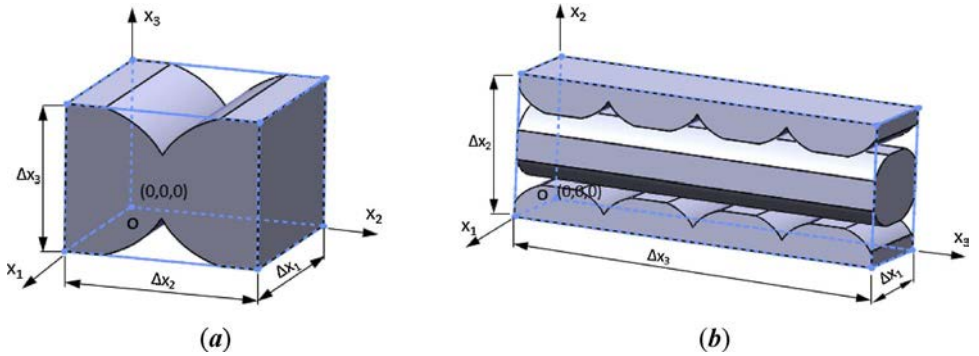

Fig. 3. The RVE of the printed plates (***a***) horizontal plate, (***b***) vertical plate.

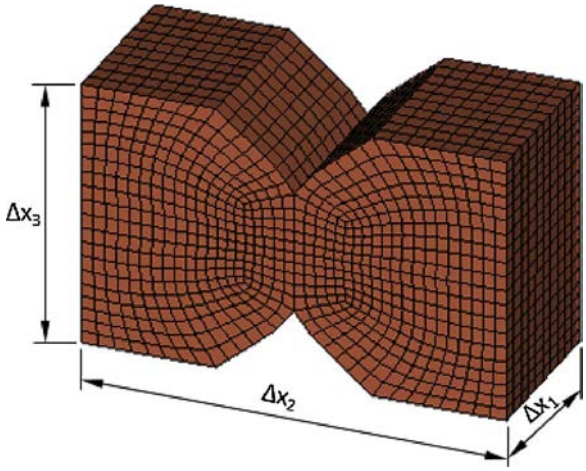

Fig. 4. The finite element model of RVE of the horizontal plate.

where $\bar{\varepsilon}_{ik}$ is average strains tensor and the first term on the right side of the Eq. (19) represents a linear distributed displacement field. The second term on the right side, $u_i^*(x_1, x_2, x_3)$, is a periodic function from one RVE to another. The periodic function u^* in the Eq. (19) is unknown and therefore, the displacement cannot be directly applied to boundaries of the RVE. These periodic boundary conditions are suitable for parallelepiped RVE models. The displacements on the pair of parallel opposite boundary surfaces is written as

$$u_i^{j+} = \bar{\varepsilon}_{ik} x_k^{j+} + u_i^* \tag{20}$$

$$u_i^{j-} = \bar{\varepsilon}_{ik} x_k^{j-} + u_i^* \tag{21}$$

where the indices $j+$ and $j-$ identify the pair of two opposite parallel boundary surfaces of a RVE. The u_i^* is same at two parallel boundaries due to periodicity, therefore, the difference between above two equations is

$$u_i^{j+} - u_i^{j-} = \bar{\varepsilon}_{ik}(x_k^{j+} - x_k^{j-}) = \bar{\varepsilon}_{ik} \triangle x_k^j \tag{22}$$

The right side of the equation becomes constant since $\triangle x_k^j$ are constants for each pair of the parallel boundary surfaces, with specified $\bar{\varepsilon}_{ik}$. These Eq. (22) are easily applicable to FE models as a nodal displacement constraint and also guarantee traction continuity condition along with displacement continuity for a periodic RVE model [37].

4. Results and discussion

This section presents the constitutive material modeling of the plates of the 3D printed L bracket structure. Initially, computation of constitutive matrix of the horizontal plate using homogenization is presented and then characterization of its material behavior using laminate constitutive relation is described. Next, vertical plate is considered for material modeling to compute its constitutive matrix. Then, the influence of build orientation of the vertical plate on the material properties is discussed. Also, effect of size of the RVE from mesostructure of the vertical plate on the material properties is investigated.

Let us take 3D printed L bracket structure via FDM with the following process parameters: lines infill pattern, 100% infill density, raster angle 0° and 90° to the *x*-axis, layer thickness 0.317 mm and 10% overlap between the adjacent fibers. The raster angle represents the printing direction of fibers in the layers and in the present case, the fibers in subsequent layers are perpendicular to each other. These process parameters define the size and orientation of the fibers in the mesostructure of the printed part and also, it is known from the literature that the mesostructure is governed by the process parameters. Consider the thickness of the plates of the L bracket structure is 3.85 mm. The cross section shape of the fiber after deposition of the material is elliptical [19,38], and length of its major axis is approximately double the minor axis and the length of minor axis is equal to the layer thickness. It is assumed in this analysis that the bonding between the fibers and layers is perfect. The filament material considered in the analysis is ABS and is one of the commonly used thermoplastic material for printing in FDM. The isotropic material properties of the ABS [7] are $E = 2230$ MPa and $\nu = 0.34$. The RVE are taken from the mesostructure of the plates and its size and shape depends on the process parameters and build orientation of the plates. The RVE is defined in local coordinate system x_1, x_2 and x_3, which are aligned in the direction of length, width and thickness of the plates, respectively. Three-dimensional continuum eight node hexahedron finite elements, C3D8, are used in the finite element modeling of RVEs and the FE modeling is done in Hypermesh (Altair Engineering) and then the homogenization is done using the micromechanics plugin in Abaqus, (Dassault Systemes). The mesh dependency is avoided by modeling RVE with smaller finite elements. The RVE is subject to six different strains, applied individually using periodic boundary conditions (Eq. (22)). That means six different load cases are prepared for six unique strains to determine the unknown elements in the constitutive matrix, *C*. The strains applied to RVE in the present analysis are $\bar{\varepsilon}_{11}$, $\bar{\varepsilon}_{22}$, $\bar{\varepsilon}_{33} = 0.01$, $\bar{\varepsilon}_{12}$, $\bar{\varepsilon}_{13}$, $\bar{\varepsilon}_{23} = 0.005$.

Now, consider the homogenization of the horizontal plate of the 3D printed structure. The dimensions of RVE are $\Delta x_1 = 0.20$, $\Delta x_2 = 0.48$, and $\Delta x_3 = 0.31$ mm. The finite element model is shown in Fig. 4. Then the FE simulation for homogenization of the material is carried out and then the unknown elements of the orthotropic constitutive matrix are calculated, as explained in section 3.1. The elements of the constitutive matrix are presented in Table 1.

Table 1
Constitutive matrix(C_{ijkl} in MPa) for the material of the 3D printed horizontal plate of the structure.

C	11	22	33	12	13	23
11	2802.7	1136.6	1150.2	0.0	0.0	0.0
22	1136.6	2299.4	1043.5	0.0	0.0	0.0
33	1150.2	1043.5	2339.6	0.0	0.0	0.0
12	0.0	0.0	0.0	674.3	0.0	0.0
13	0.0	0.0	0.0	0.0	678.0	0.0
23	0.0	0.0	0.0	0.0	0.0	637.8

Table 2
The elastic moduli (E_i, G_{ij} in MPa) for the material of the 3D printed horizontal plate.

	Numerical		Experimental			
	Present	Ref. [39]	Ref. [7]	Ref. [33]	Ref. [34]	Ref. [40]
E_1	202-5.1	1851.9	2030.9	1972	1790	1810
E_2	166-0.2	1501.3	1251.6	1762	1150	1695
E_3	168-6.4					
G_{12}	674.-3	625.4	410.0	676	808.5	617
G_{13}	678.-0					
G_{23}	637.-8					
ν_{12}	0.34	0.34	0.39	0.37	0.34	0.32
ν_{13}	0.34					
ν_{23}	0.30					

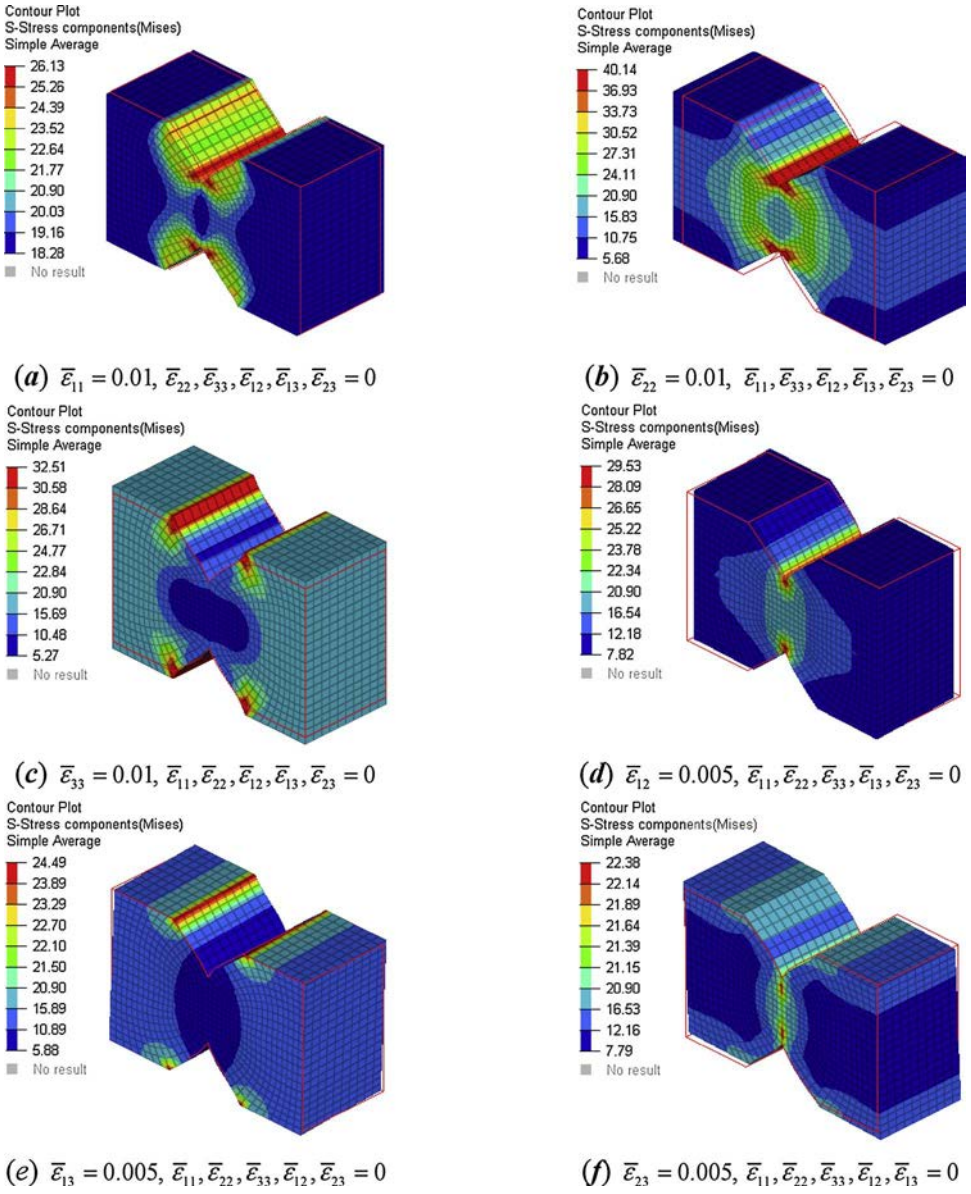

Fig. 5. Stress contours in RVE of the horizontal plate subjected to different strains.

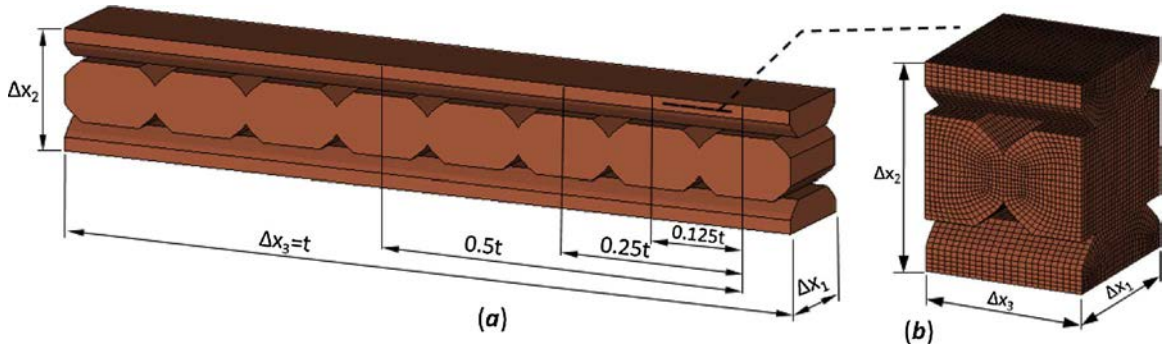

Fig. 6. RVE of the vertical plate, (***a***) Δx_3 equal to thickness of plate, t (***b***) Δx_3 equal to 0.125t.

The elastic moduli of the orthotropic material can be calculated from constitutive matrix using Eq. (3) and the elastic moduli for the 3D printed horizontal plate are provided in the Table 2. The present results using numerical homogenization are compared with the elastic moduli available in the literature from experimental work by the researchers in the Table 2. The elastic moduli from the experimental work can only be useful for constitutive matrix of the plane stress case of the 3D printed structures. The present analysis results are comparable with results of the experimental work. The difference in the experimental results by the researchers is mainly due to the process parameters employed during printing of the test coupons. The layer thickness and the overlap between adjacent fibers are the major process parameters which vary,

Table 3
Constitutive matrix (C_{ijkl} in MPa) of the 3D printed vertical plate of the structure, for Δx_3 of RVE is 0.125*t*.

C	11	22	33	12	13	23
11	2290.3	684.6	627.8	0.0	0.0	0.0
22	684.6	1589.7	508.1	0.0	0.0	0.0
33	627.8	508.1	1456.1	0.0	0.0	0.0
12	0.0	0.0	0.0	561.6	0.0	0.0
13	0.0	0.0	0.0	0.0	538.0	0.0
23	0.0	0.0	0.0	0.0	0.0	491.1

Table 4
Constitutive matrix (C_{ijkl} in MPa) of the vertical plate of the structure, for Δx_3 of RVE is 0.25*t*.

C	11	22	33	12	13	23
11	2337.2	717.9	742.6	0.0	0.0	0.0
22	717.9	1617.9	593.5	0.0	0.0	0.0
33	742.6	593.5	1745.2	0.0	0.0	0.0
12	0.0	0.0	0.0	562.7	0.0	0.0
13	0.0	0.0	0.0	0.0	600.8	0.0
23	0.0	0.0	0.0	0.0	0.0	526.0

among those experimental studies. The variation in the present analysis results and experimental is due to that the mesostructure represented in the present FE model is not exact replication of the mesostructure exist in the test coupons of experiments. Also, it is assumed in this work that the bonding between the adjacent fibers is prefect, but it is not true in the printed coupons. However, the present analysis is an alternate to experimental work and provides accurate results compare to that of experimental work. Furthermore, this analysis gives the all nine independent elements of ***C*** matrix unlike experimental work.

Six different load cases of RVE subjected to six unique strains are simulated for the analysis and the stress contours of the RVE for

Table 5
Constitutive matrix (C_{ijkl} in MPa) of the vertical plate of the structure, for Δx_3 of RVE is 0.5*t*.

C	11	22	33	12	13	23
11	2383.5	751.0	857.4	0.0	0.0	0.0
22	751.0	1643.8	677.5	0.0	0.0	0.0
33	857.4	677.5	2033.3	0.0	0.0	0.0
12	0.0	0.0	0.0	563.3	0.0	0.0
13	0.0	0.0	0.0	0.0	640.8	0.0
23	0.0	0.0	0.0	0.0	0.0	544.2

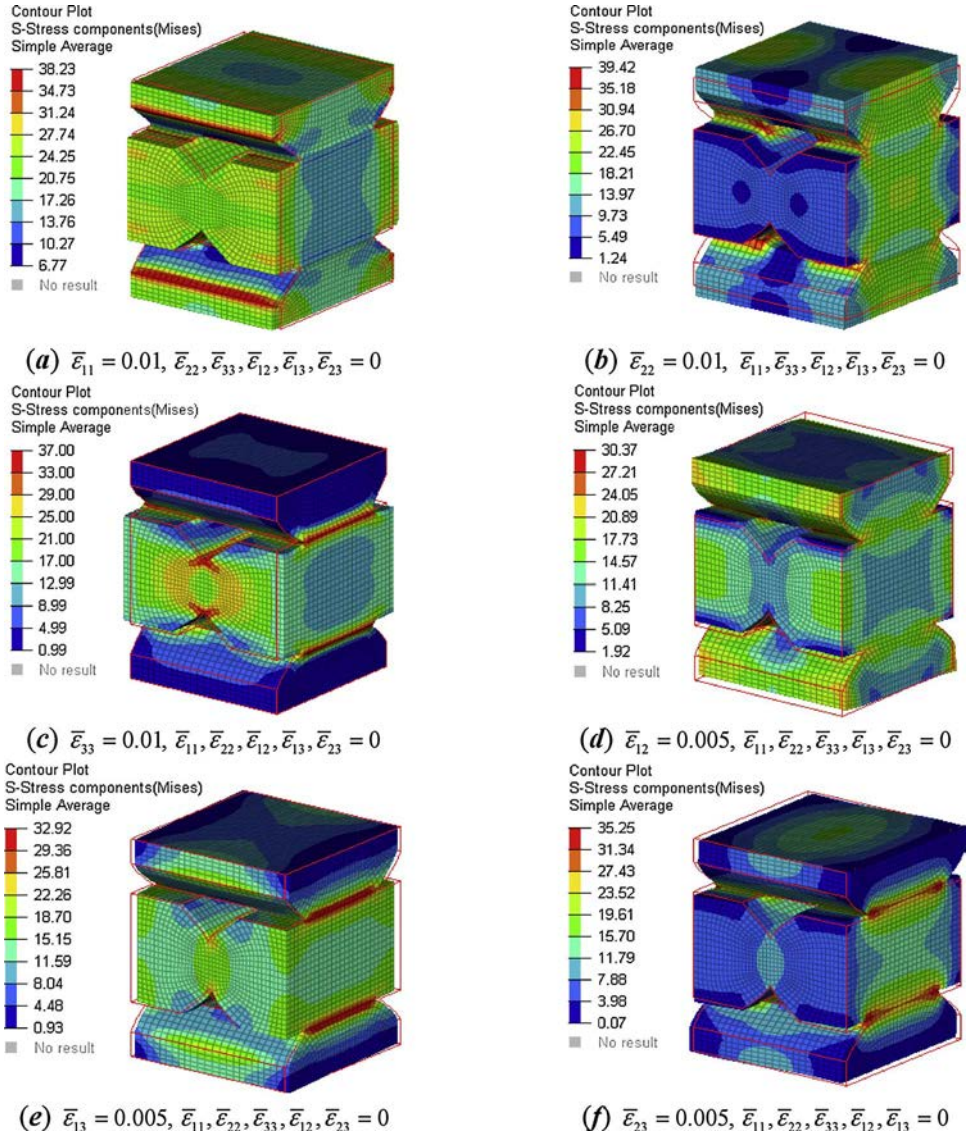

Fig. 7. Stress contours in the RVE of $\Delta x_3 = 0.125\,t$ of the vertical plate subjected to different strains.

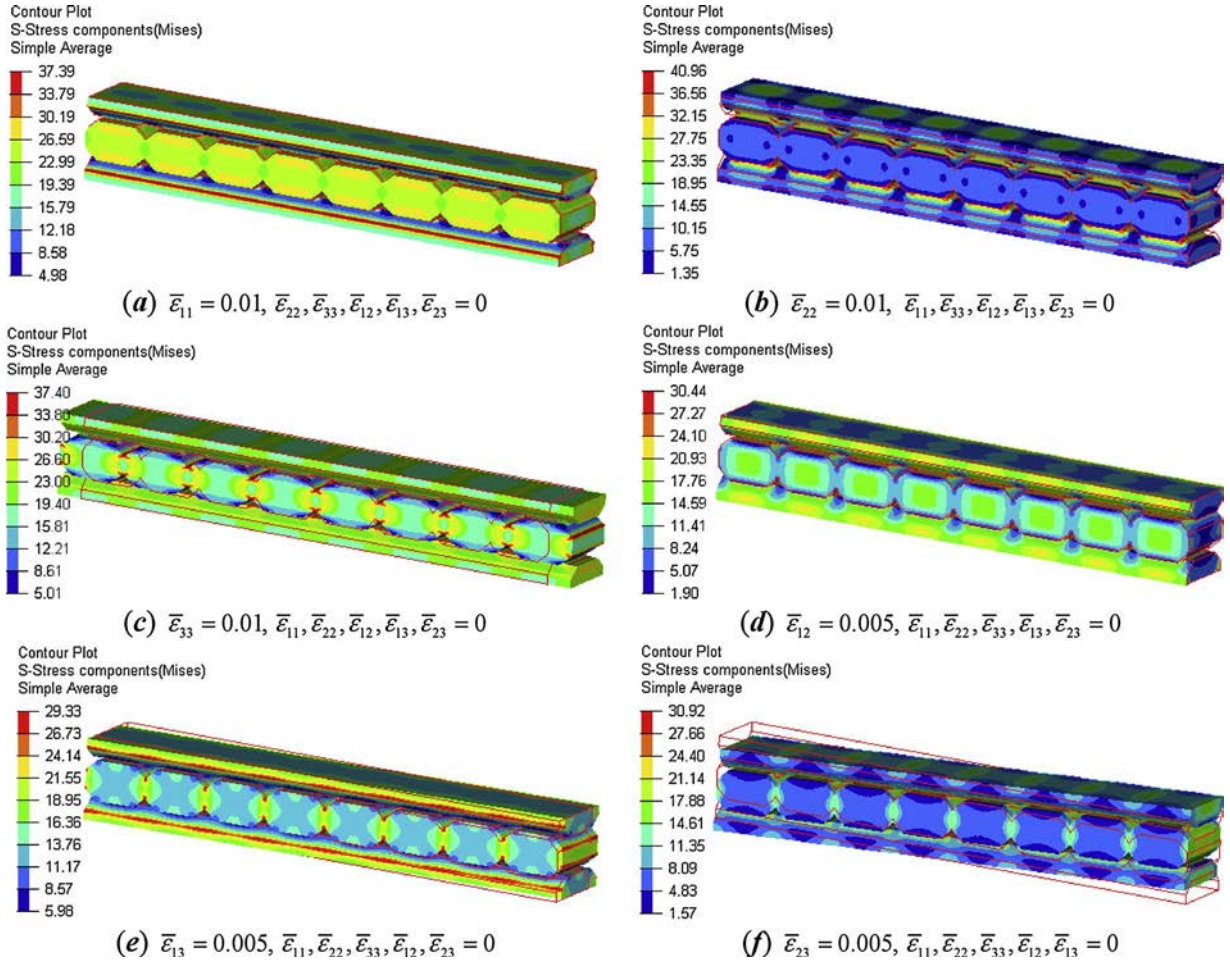

Fig. 8. Stress contours in the RVE of $\Delta x_3 = t$ of the vertical plate subjected to different strains.

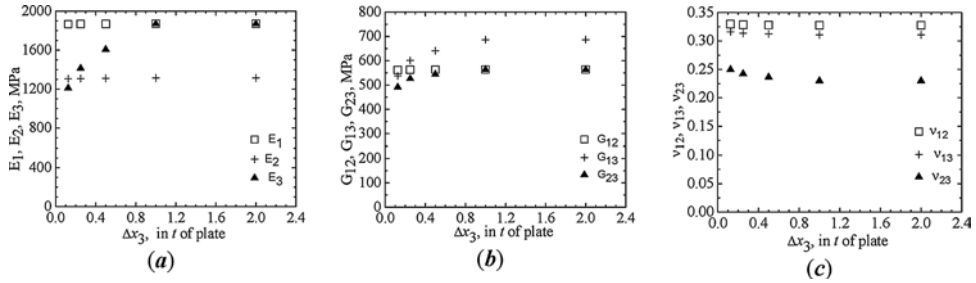

Fig. 9. Variation in the elastic moduli of the material of the vertical plate for different values of Δx_3 of RVE, (***a***) $E - \Delta x_3$, (***b***) $G - \Delta x_3$ and (***c***) $\nu - \Delta x_3$.

Table 6
Constitutive matrix (C_{ijkl} in MPa) of the vertical plate, for Δx_3 of RVE equal to 1.0 t and 2t.

C	11	22	33	12	13	23
11	2450.3	799.0	1023.5	0.0	0.0	0.0
22	799.0	1680.6	798.9	0.0	0.0	0.0
33	1023.5	798.9	2450.3	0.0	0.0	0.0
12	0.0	0.0	0.0	563.8	0.0	0.0
13	0.0	0.0	0.0	0.0	686.7	0.0
23	0.0	0.0	0.0	0.0	0.0	563.7

different load cases are shown in Fig. 5. The maximum stress in all deformation cases is occurring at interface of the fibers and is because of the less material present at the interface. Therefore, the weakest section in the mesostructure is the interface and it is more prone to initiation of the crack during the loading. The stress is higher in the case of applied strain $\bar{\varepsilon}_{22} \neq 0$ and is occurring at the interface of the fibers. Therefore, debonding between the fibers can occur due of such loads and this phenomenon ultimately could lead to failure of the 3D printed parts.

The material behavior of the horizontal plate is characterized using the constitutive relation of the laminate, Eq. (8). It accounts the printing direction and layer thickness for the constitutive material behavior of the printed part. The thickness of layers is 0.317 mm in the horizontal plate of 3.85 mm thick and therefore, the number of layers in the plate would be 12 of equal thickness. Then the stacking sequence of the layers with defined raster angle in the horizontal plate is $[0^\circ/90^\circ]_6$. The horizontal plate behaves as laminate and therefore, the constitutive relation of laminate can be used in the mechanical behavior characterization of the plate using classical laminate theory [39].

Next, let us consider the constitutive material modeling of the 3D printed vertical plate of the L bracket structure using homogenization.

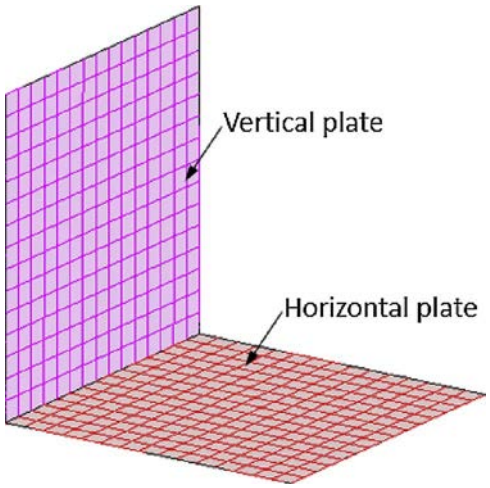

Fig. 10. Finite element model of L bracket structure for stress analysis.

The build orientation of this plate is *upright* and is different from the horizontal plate, which is *flat*. As explained earlier, that the mechanical properties of the printed part are influenced by build orientation. Consider that the thickness of this plate is same as thickness of the horizontal plate, 3.85 mm. The RVE of the plate is taken from the mesostructure of the vertical plate is shown in Fig. 6. The Fig. 6a represents the different length of dimension Δx_3 of RVE from the mesostructure of the vertical plate.

Let us consider the RVE shown in Fig. 6b; it has the fibers of three adjacent layers, oriented perpendicular to each other. Its architecture is different from the RVE of horizontal plate, which represents only single layer. It is because the layers of the plate do not act as laminae and therefore, laminate theory cannot be employed for this plate as explained earlier. The RVE represents the direction of the fibers in the subsequent layers and their thickness. Further, it accounts the effect of build orientation of the layers of the plate. The dimensions of RVE are $\Delta x_1 = 0.48$, $\Delta x_2 = 0.62$, and $\Delta x_3 = 0.48$ mm. The FE model of the RVE, shown in Fig. 6b, is simulated for six different load cases. Then the unknown elements of orthotropic constitutive matrix are calculated and are presented in the Table 3.

The stress contours and the deformation modes of the RVE subjected to six unique strains are shown in Fig. 7. In all deformation modes, the maximum stress is at the interface of fibers. The deformation mode of the case $\bar{\varepsilon}_{22} \neq 0$ is more prone to initiate the crack at the interface of the fibers because of the highest stress is seen in this case. The RVE of the horizontal plate is taken from a single layer and therefore the dimension, Δx_3, of the RVE is equal to the thickness of the layer. Whereas, the dimension Δx_3 of the RVE in the thickness direction of the vertical plate affects the constitutive matrix of the plate and its influence is investigated in the following work. Different sizes of RVE such as $\Delta x_3 = 0.25t$, $0.50\,t$ and t, as seen in Fig. 6a, are taken from the vertical plate for the investigation. Then, these FE models of RVE are simulated for different load cases and then the computed constitutive matrix are presented in Tables 4–6. Further to study its influence on thicker plates, the simulations are also performed for $\Delta x_3 = 2\,t$ case and the obtained results are same as previous case ($\Delta x_3 = t$).

From the results presented in Tables 4–6, it can be seen that the increase in the values of the C_{1133}, C_{2233}, C_{3333}, C_{1313}, C_{2323} of the C matrix with increase in the Δx_3. It is clear that the stiffness values in the direction 3 of the coordinate system for the RVE of the vertical plate are influenced with variation of Δx_3 until its value equal to thickness (t) of the plate. Further increase of Δx_3 above the thickness of the plate does not affect the constitutive matrix, as seen that the element of C matrix in Table 6 are same for $\Delta x_3 = t$ and $2t$. The stress contours of the RVE with $\Delta x_3 = t$ subjected to different strains are shown in the Fig. 8.

The elastic moduli can be calculated using Eq. (3) for the orthotropic constitutive matrices presented in Tables 4–6. The variation in the elastic moduli of the material of the 3D printed vertical plate for different dimensions of Δx_3 of RVE are shown in Fig. 9. The elastic moduli such as E_3, G_{13}, G_{23}, ν_{13} and ν_{23} values are improved with increase of Δx_3 until it equals to thickness of the plate. So it is clear from this study that the selection of Δx_3 of the RVE for homogenization of the material of the plate printed in *upright* orientation is important in defining the constitutive matrix of the plate. Furthermore, the constitutive matrices of the horizontal and vertical plate presented in the Tables 1 and 6 are not same due to their build orientation in the structure. It can be noted that the constitutive matrix computed from RVE of $\Delta x_3 = t$ and also $2\,t$ is transversely isotropic constitutive matrix, where two of E, G and ν are same. In all other cases, the constitutive matrix is orthotropic. That means the thickness of the plate printed in *upright* orientation can change the constitutive behavior of the plate, *i.e* orthotropic to transversely isotropic. The constitutive material behavior of the parts printed with *edge* build orientation would be similar to that of parts with *upright* build orientation, since layers deposition is across the thickness of the part in both case.

Now consider the finite element modeling of 3D printed L bracket structure for stress analysis. Two dimensional finite element mesh on the mid-surfaces of the plates of the structure, shown in Fig. 10, is used for stress analysis. The constitutive matrix of the plates is considered to account for their material behavior during the analysis. The effective constitutive matrix of the plates is chosen based on their build orientation and thickness for design and analysis of the structure subjected to different loads. The Table 7 presents the constitutive matrix of the plates of the L bracket structure based on their build orientation and thickness.

5. Conclusions

The constitutive material behavior of the different parts of 3D printed structure is not the same and the behavior depends on the build orientation of the parts of the structure. The material behavior of parts of the structure printed in *flat* build orientation can be characterized using laminate constitutive relation during the stress analysis of the structure. The parts of the structure printed in *upright* and *edge* build orientation cannot be characterized using laminate theory. The material behavior of the parts with such build orientations is orthotropic and therefore, constitutive relation of orthotropic material is employed for characterizing their behavior during the analysis of the structure. Although an isotropic filament material is used for printing the structure, the final constitutive behavior of the part is not same as original filament material. Then the computation of the constitutive matrix of the printed parts using numerical homogenization technique is

Table 7
Constitutive matrices for the plates of the L bracket structure.

Parts of structure	Horizontal	Vertical plate				
Build orientation	*Flat*	*Upright*				
Thickness, t mm	4	0.5	1.0	2	4	8
C matrix	Table 1	Table 3	Table 4	Table 5	Table 6	
Behavior	Laminate	Orthotropic	Orthotropic	Orthotropic	Transversely isotropic	

presented. The constitutive matrix of the parts of the structure oriented differently are computed. Furthermore, influence of build orientation of the parts of the structure on the constitutive material behavior is investigated. The computed stiffness values of constitutive matrix from the analysis is different for *upright* and *flat* build orientation of the part of same thickness. It is revealed that the thickness of the part printed in *upright* and *edge* orientation also influence its constitutive material behavior. It was found that with increase in thickness of the part printed in *upright* and *edge* build orientation their material behavior changes from orthotropic to transversely isotropic. So, it is very important to consider final constitutive material behavior of the parts of the 3D printed structure with different build orientations for effective design and analysis of the structure.

Acknowledgments

The authors would like to thank Julian and Roger Carrick for proof reading the manuscript. This research did not receive any specific grant from funding agencies in the public, commercial, or not-for-profit sectors.

References

[1] D.L. Bourell, Perspectives on additive manufacturing, Annu. Rev. Mater. Res. 46 (2016) 1–18.
[2] N. Guo, M.C. Leu, Additive manufacturing: technology, applications and research needs, Front. Mech. Eng. 8 (3) (2013) 215–243.
[3] General Electric, Annual Report (2016). http://www.ge.com/ar2016/assets/pdf/GE_AR16.pdf.
[4] J. Kotlinski, Mechanical properties of commercial rapid prototyping materials, Rapid Prototyp. J. 20 (6) (2014) 499–510.
[5] P. Kulkarni, D. Dutta, Deposition strategies and resulting part stiffnesses in fused deposition modeling, J. Manuf. Sci. Eng. 121 (1) (1999) 93–103.
[6] M.K. Agarwala, V.R. Jamalabad, N.A. Langrana, A. Safari, P.J. Whalen, S.C. Danforth, Structural quality of parts processed by fused deposition, Rapid Prototyp. J. 2 (4) (1996) 4–19.
[7] L. Li, Q. Sun, Composite modeling and analysis for fabrication of FDM prototypes with locally controlled properties, J. Manuf. Process. 4 (2002) 129–141.
[8] S.H. Ahn, M. Montero, D. Odell, S. Roundy, P.K. Wright, Anisotropic material properties of fused deposition modeling ABS, Rapid Prototyp. J. 8 (4) (2002) 248–257.
[9] M. Dawoud, I. Taha, S.J. Ebeid, Mechanical behaviour of ABS: An experimental study using FDM and injection moulding techniques, J. Manuf. Process. 21 (2016) 39–45.
[10] F. Ning, W. Cong, Y. Hu, H. Wang, Additive manufacturing of carbon fiber reinforced plastic composites using fused deposition modeling: effects of process parameters on tensile properties, J. Compos. Mater. 51 (4) (2017) 451–462.
[11] C. Ziemian, M. Sharma, S. Ziemian, Anisotropic Mechanical Properties of ABS Parts Fabricated by Fused Deposition Modelling, InTech, 2012.
[12] J.C. Riddick, M.A. Haile, R. Von Wahlde, D.P. Cole, O. Bamiduro, T.E. Johnson, Fractographic analysis of tensile failure of acrylonitrile butadiene styrene fabricated by fused deposition modeling, Addit. Manuf. 11 (2016) 49–59.
[13] S. Ziemian, M. Okwara, C.W. Ziemian, Tensile and fatigue behavior of layered acrylonitrile butadiene styrene, Rapid Prototyp. J. 21 (3) (2015) 270–278.
[14] B. Huang, S. Singamneni, Raster angle mechanics in fused deposition modelling, J. Compos. Mater. 49 (3) (2015) 363–383.
[15] D. Jiang, D.E. Smith, Anisotropic mechanical properties of oriented carbon fiber filled polymer composites produced with fused filament fabrication, Addit. Manuf. 18 (2017) 84–94.
[16] J. Torres, J. Cotelo, J. Karl, A.P. Gordon, Mechanical property optimization of FDM PLA in shear with multiple objectives, JOM 67 (5) (2015) 1183–1193.
[17] B. Rankouhi, S. Javadpour, F. Delfanian, T. Letcher, Failure analysis and mechanical characterization of 3D printed ABS with respect to layer thickness and orientation, J. Fail. Anal. Prev. 16 (3) (2016) 467–481.
[18] C. Bellehumeur, L. Li, Modeling of bond formation between polymer filaments in the fused deposition modeling process, J. Manuf. Process. 6 (2) (2004) 170–178.
[19] Q. Sun, G.M. Rizvi, C.T. Bellehumeur, P. Gu, Effect of processing conditions on the bonding quality of FDM polymer filaments, Rapid Prototyp. J. 14 (2) (2008) 72–80.
[20] A. Bellini, S. Güçeri, Mechanical characterization of parts fabricated using fused deposition modeling, Rapid Prototyp. J. 9 (4) (2003) 252–264.
[21] M. Domingo-Espin, J.M. Puigoriol-Forcada, A.A. Garcia-Granada, J. Llumà, S. Borros, G. Reyes, Mechanical property characterization and simulation of fused deposition modeling Polycarbonate parts, Mater. Des. 83 (2015) 670–677.
[22] K. Thrimurthulu, P.M. Pandey, N.V. Reddy, Optimum part deposition orientation in fused deposition modeling, Int. J. Mach. Tools Manuf. 44 (6) (2004) 585–594.
[23] P. Delfs, M. Ťows, H.J. Schmid, Optimized build orientation of additive manufactured parts for improved surface quality and build time, Addit. Manuf. 12 (2016) 314–320.
[24] T.D. McLouth, J.V. Severino, P.M. Adams, D.N. Patel, R.J. Zaldivar, The impact of print orientation and raster pattern on fracture toughness in additively manufactured ABS, Addit. Manuf. 18 (2017) 103–109.
[25] Martínez,, Modelization and structural analysis of FDM parts, AIP Conf. Proc. 2012 (1431) 842–848.
[26] I. Durgun, R. Ertan, Experimental investigation of FDM process for improvement of mechanical properties and production cost, Rapid Prototyp. J. 20 (3) (2014) 228–235.
[27] C.W. Ziemian, R.D. Ziemian, K.V. Haile, Characterization of stiffness degradation caused by fatigue damage of additive manufactured parts, Mater. Des. 109 (2016) 209–218.
[28] J.T. Cantrell, S. Rohde, D. Damiani, R. Gurnani, L. DiSandro, J. Anton, A. Young, A. Jerez, D. Steinbach, C. Kroese, P.G. Ifju, Experimental characterization of the mechanical properties of 3D-printed ABS and polycarbonate parts, Rapid Prototyp. J. 23 (4) (2017) 811–824.
[29] R.J. Zaldivar, D.B. Witkin, T. McLouth, D.N. Patel, K. Schmitt, J.P. Nokes, Influence of processing and orientation print effects on the mechanical and thermal behavior of 3D Printed ULTEM® 9085 Material, Addit. Manuf. 13 (2017) 71–80.
[30] Y.T. Kao, Y. Zhang, J. Wang, B.L. Tai, Bending behaviors of 3D-printed Bi-material structure: experimental study and finite element analysis, Addit. Manuf. (2017), http://dx.doi.org/10.1016/j.addma.2017.06.005.
[31] A. Garg, A. Bhattacharya, An insight to the failure of FDM parts under tensile loading: finite element analysis and experimental study, Int. J. Mech. Sci. 120 (2017) 225–236.
[32] M.R. Karamooz Ravari, M. Kadkhodaei, M. Badrossamay, R. Rezaei, Numerical investigation on mechanical properties of cellular lattice structures fabricated by fused deposition modeling, Int. J. Mech. Sci. 88 (2014) 154–161.
[33] J.F.A. Rodriguez James, P. Thomas, J.E. Renaud, Mechanical behavior of acrylonitrile butadiene styrene (ABS) fused deposition materials, Exp. Investig. Rapid Prototyp. J. 7 (3) (2001) 148–158.
[34] C. Casavola, A. Cazzato, V. Moramarco, C. Pappalettere, Orthotropic mechanical properties of fused deposition modelling parts described by classical laminate theory, Mater. Des. 90 (2016) 453–458.
[35] R.H. Hambali, H.K. Celik, P.C. Smith, A.E.W. Rennie, M. Ucar, Effect of build orientation on FDM parts: a case study for validation of deformation behaviour by FEA, In Proc, iDECON (2010) 224–228.
[36] S.J. Hollister, N. Kikuchi, A comparison of homogenization and standard mechanics analyses for periodic porous composites, Comput. Mech. 10 (2) (1992) 73–95.
[37] Z. Xia, Y. Zhang, F. Ellyin, A unified periodical boundary conditions for representative volume elements of composites and applications, Int. J. Solids Struct. 40 (8) (2003) 1907–1921.
[38] H.L. Tekinalp, V. Kunc, G.M. Velez-Garcia, C.E. Duty, L.J. Love, A.K. Naskar, C.A. Blue, S. Ozcan, Highly oriented carbon fiber-polymer composites via additive manufacturing, Compos. Sci. Technol. 105 (2014) 144–150.
[39] M. Somireddy, A. Czekanski, Mechanical characterization of additively manufactured parts by FE modeling of mesostructure, J. Manuf. Mater. Process. 1 (2) (2017) 18.
[40] G. Alaimo, S. Marconi, L. Costato, F. Auricchio, Influence of meso-structure and chemical composition on FDM 3D-printed parts, Compos. Part B Eng. 113 (2017) 371–380.